Supported Organometallic Complexes. XXXVI [1]

Diaminediphosphineruthenium(II) Interphase Catalysts for the Hydrogenation of α,β-Unsaturated Ketones

Ekkehard Lindner[a,*], Samer Al-Gharabli[a], Ismail Warad[a], Hermann A. Mayer[a], Stefan Steinbrecher[b], Erich Plies[b], Michael Seiler[c], and Helmut Bertagnolli[c]

Tübingen, [a] Institut für Anorganische Chemie und [b] Institut für Angewandte Physik der Universität
[c] Stuttgart, Institut für Physikalische Chemie der Universität

Received September 17th 2002.

Dedicated to Professor Dieter Fenske on the Occasion of his 60th Birthday

Abstract. The T−silyl functionalized diamine-bis(ether-phosphine)ruthenium(II) complexes **1a(T°)** − **1g(T°)** (Scheme 1) were sol-gel processed in the presence of different amounts of the co-condensation agents $CH_3Si(OMe)_3$ **(Me−T°)** and $(MeO)_2SiMe-(CH_2)_6-MeSi(OMe)_2$ **(D°−C_6−D°)** to produce a library of the interphase catalysts **X1a − X1c**, **X2a − X2g**, and **X3a − X3g**. Due to the remarkable electronic and steric effects of the co-ligands on the catalytic activity of such complexes, a series of aliphatic and aromatic diamines was selected. The new polymers were investigated by multinuclear CP/MAS solid-state NMR spectroscopy as well as by EXAFS, EDX, SEM, and BET methods. Selected interphase catalysts show high activities and selectivities in the hydrogenation of *trans*-4-phenyl-3-butene-2-one.

Keywords: Heterogenization; Phosphines; Amines; Sol-gel process; NMR (solid state) spectroscopy; EDX; EXAFS; Catalysis

Diamindiphosphinruthenium(II)-Interphasen-Katalysatoren für die Hydrierung von α,β-ungesättigten Ketonen

Inhaltsübersicht. Die T-silyl-funktionalisierten Diamin-bis(etherphosphin)ruthenium(II) Komplexe **1a(T°) − 1g(T°)** (Schema 1) wurden mit unterschiedlichen Mengen der Cokondensationsmittel $CH_3Si(OMe)_3$ **(Me−T°)** und $(MeO)_2SiMe-(CH_2)_6-MeSi(OMe)_2$ **(D°−C_6−D°)** Sol-Gel-prozessiert, um eine Bibliothek der Interphasen-Katalysatoren **X1a − X1c**, **X2a − X2g** und **X3a − X3g** zu erhalten. Wegen des bemerkenswerten elektronischen und sterischen Einflusses der Coliganden auf die katalytische Aktivität solcher Komplexe, wurde eine Reihe von aliphatischen und aromatischen Diaminen gewählt. Die neuen Polymeren wurden durch Multikern-CP/MAS-Festkörper-NMR-Spektroskopie und mit Hilfe von EXAFS-, EDX-, SEM- und BET-Methoden untersucht. Ausgewählte Interphasen-Katalysatoren zeigen hohe Aktivitäten und Selektivitäten bei der Hydrierung von *trans*-4-Phenyl-3-buten-2-on.

Introduction

An intermediate step between combinatorial chemistry [2−5], which is well established in pharmaceutical industry, and traditional synthesis is parallel synthesis [6]. This methodology has received considerable attention for materials science and catalysis [7−9]. In a recent paper [10], we have been concerned with the development of a synthetic route to an array of important neutral and cationic diamine-bis-(ether-phosphine)ruthenium(II) complexes. Compounds of this type are potential candidates for the application of parallel methods in catalysis, since they are active in the catalytic hydrogenation of unsaturated ketones [11−13]. Subsequent studies now are oriented to the combination of interphase chemistry and parallel synthesis. Meanwhile interphase catalysts [14] have attained a remarkable importance since they are able to combine the advantages of homogeneous and heterogeneous catalysis with a considerable reduction of notorious drawbacks like leaching and limited catalytic activity of the reactive centers [14,15].

Interphases are systems in which a stationary phase (e.g. a reaction center linked to a matrix via a spacer) and a mobile component (e.g. a gaseous, liquid, or dissolved reactant) penetrate each other on a molecular scale without forming a homogeneous phase. If such interphases are provided with a swellable polymer, they are able to imitate homogeneous conditions, because the active centers become highly mobile simulating the properties of a solution and hence they are accessible for substrates. In a preceding investigation the above-mentioned diamine-bis(ether-phosphine)ruthenium(II) complexes [10] were provided with spacer functions at the periphery of the phosphine ligands

* Prof. Dr. Ekkehard Lindner
Institut für Anorganische Chemie II der Universität Tübingen
Auf der Morgenstelle 18
D−72076 Tübingen
Tel.: (+) 49 7071 2972039
Fax: (+) 49 7071 295306.
E-Mail: ekkehard.lindner@uni-tuebingen.de

Table 1 Labeling of the Compounds

Ruthenium complex[a)]	Co-condensation agent	Ideal T:D or T:T′ ratio[b)]	Compound	Xerogel
1a(T°)−1c(T°)	**D°−C_6−D°**	1:10	**1a, b, c(T^n)(D^i−C_6−D^i)$_{10}$**	**X1a, X1b, X1c**
1a(T°)−1g(T°)	**Me-T°**	1:5	**1a−g(T^n)(Me-T^i)$_{10}$**	**X2a−X2g**
1a(T°)−1g(T°)	**Me-T°**	1:10	**1a−g(T^n)(Me-T^i)$_{20}$**	**X3a−X3g**

[a)] See Scheme 1. [b)] T and T′ refer to the complex and co-condensation agent, respectively.

with hydrolyzable T-silyl groups at their ends [16]. In continuation of our work we now wish to report on the poly-co-condensation of a set of T-silyl functionalized diamine-bis(ether-phosphine)ruthenium(II) complexes with a different amounts of $(MeO)_2SiMe(CH_2)_6MeSi(OMe)_2$ (**D°−C_6−D°**) and $MeSi(OMe)_3$ (**Me−T°**), respectively. In a recent paper it was demonstrated that a variation of the T:D ratios leads to an optimization of the mobility of polymeric materials which is accompanied by an improvement of the catalytic activity of the polymeric catalysts [17]. On the other hand from fluorescence spectroscopic investigations it was deduced that **Me−T^n** hybrid polymers reveal a high mobility in the swollen state [18]. For this reason the above-mentioned co-condensation agents were selected. An indispensable technique to characterize these polymeric materials is solid-state NMR spectroscopy. Some of the hybrid catalysts were also exemplarily probed by EXAFS, EDX, SEM, and BET measurements. These new stationary phases represent valuable examples for further studies regarding a parallel testing of the catalytic activity in the selective hydrogenation of unsaturated ketones.

Results and Discussion

Sol−Gel Processing

For the access of reproducible polymeric materials uniform reaction conditions have to be maintained. The properties of the sol-gel processed products strongly depend on reaction conditions like type of solvent, kind of catalyst, concentration of the monomers, reaction time, and temperature [19]. All polycondensations were performed in a mixture of THF/MeOH with an excess of water and $(n\text{-Bu})_2Sn(OAc)_2$ as catalyst. The alcohol is necessary to homogenize the reaction mixture. Sol-gel processes were carried out at ambient temperature in the presence of the two co-condensation agents **D°−C_6−D°** and **Me−T°**.

Two kinds of stationary phases were obtained: (i) xerogels **X1a − X1c** were synthesized by co-condensation of **1a(T°) − 1c(T°)** with **D°−C_6−D°** (Scheme 1); (ii) xerogels **X2a − X2g** and **X3a − X3g** were formed by co-condensation of **1a(T°) − 1g(T°)** with two different amounts of **Me−T°** (T : T′ = 1 : 5 and 1 : 10, respectively) (Scheme 1 and Table 1).

Solid-State NMR Spectroscopic Investigations

Due to cross-linking effects the solubility of the polymeric materials **X1a − X1c**, **X2a − X2g**, and **X3a − X3g** is rather limited. Therefore solid-state NMR spectroscopy was used as a powerful technique for their characterization.

^{29}Si CP/MAS NMR Spectroscopy

As demonstrated in Figure 1, the ^{29}Si CP/MAS NMR spectra of the different materials show signals for substructures corresponding to D^i and T^n functions.The average chemical shifts for D° (δ = −2.2), D^1 (δ = −13.4), D^2 (δ = −22.5), T^2 (δ = −58.0), and T^3 (δ = −65.3) species are not significantly changed by the incorporation of different amounts of the co-condensation agents **D^i−C_6−D^i** and **Me−T^n** and are in agreement with values reported in the literature for similar systems [20]. Since all silicon atoms are in direct proximity of protons the *Hartmann-Hahn* [21] match could efficiently be achieved. This allows the cross polarization method to be adapted for ^{29}Si solid-state NMR spectroscopic investigations.

The employment of **D°−C_6−D°** in the sol-gel process leads to a high degree of condensation for all D-type polymers. Overlapping ^{29}Si resonances of the T-subgroups in the spectra of **X2a − X2g** and **X3a − X3g** prevent the calculation of the degree of condensation. T^1 and T^2 signals represent very low intensity indicating also a high degree of cross-linking.

^{13}C and ^{31}P CP/MAS NMR Spectroscopy

In the ^{13}C CP/MAS NMR spectra of the supported complexes **X1a − X1c**, **X2a − X2g**, and **X3a −X3g** characteristic peaks at approximately δ = −0.3 and −3.8 are assigned to the carbon atoms of the silicon adjacent methyl groups in the Si−O−Si substructure of the poly-co-condensates **D^i−C_6−D^i** and **Me−T^n**, respectively (Figure 2). As a consequence of the sol-gel process, resulting in the formation of hybrid polymers, the carbon nuclei of the silicon neighboring methylene functions are shifted to lower field of about 5 ppm compared to the monomeric starting compounds. In some of the spectra only weak ^{13}C signals were assigned to residual Si−OR functionalities which point to a high degree of hydrolysis [21].

All ^{31}P resonances in the ^{31}P CP/MAS NMR spectra of **X1a − X1c**, **X2a − X2g**, and **X3a −X3g** are found in the expected ranges and are broadened due to the chemical shift dispersion (Figure 3) [21].

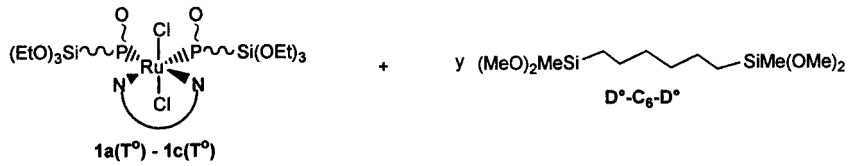

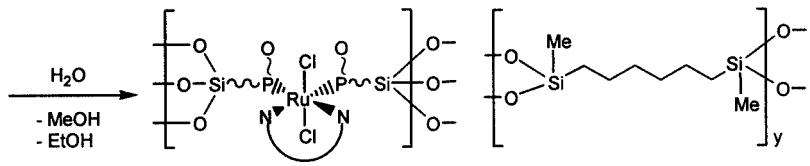

Idealized polycondensation: **1a,b,c** $(T^3)(D^2\text{-}C_6\text{-}D^2)_y$; y = 10 (**1**)
Realistic composition: **1a,b,c** $(T^n)(D^i\text{-}C_6\text{-}D^i)_y$ (**X1a, X1b, X1c**)

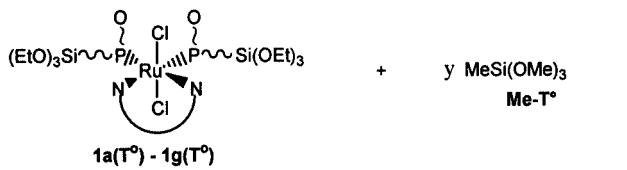

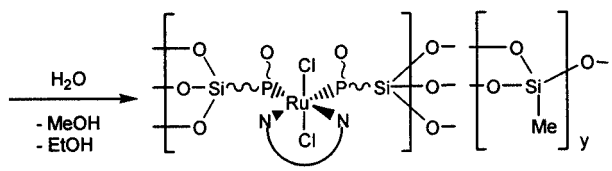

Idealized polycondensation: **1a - g** $(T^3)(Me\text{-}T^3)_y$; y = 10 (**2**), 20 (**3**)
Realistic composition: **1a - g** $(T^n)(Me\text{-}T^n)_y$ (**X2a - X2g, X3a - X3g**)

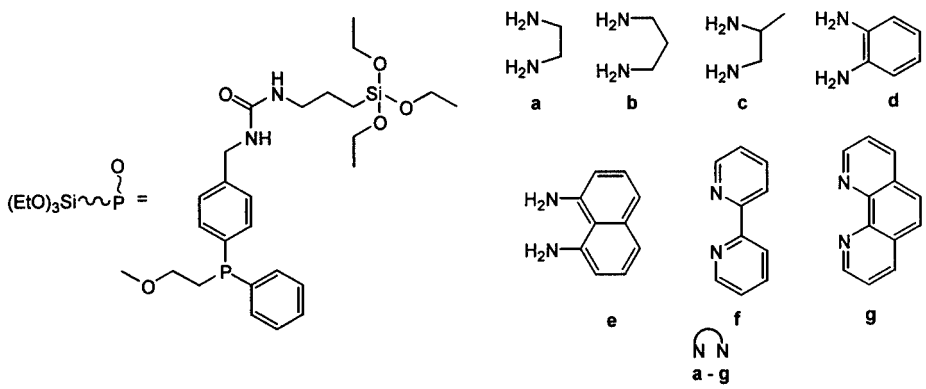

T = T type of silicon atom (three oxygen neighbors)
D = D type of silicon atom (two oxygen neighbors)
i, n = numbers of Si-O-Si bonds (i = 0-2; n = 0-3)

Scheme 1 Structures, idealized, and realistic compositions of the xerogels **X1a−X1c, X2a−X2g,** and **X3a−X3g**.

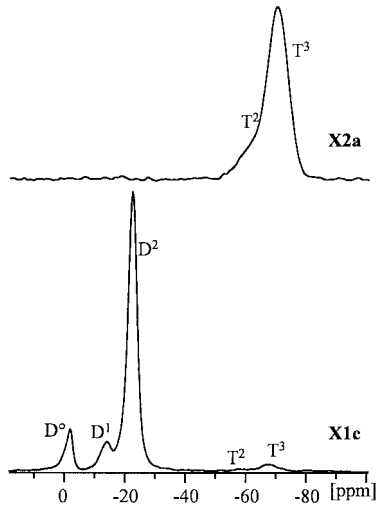

Fig. 1 ^{29}Si CP/MAS NMR spectra of the polymeric materials **X1c** and **X2a** (selected).

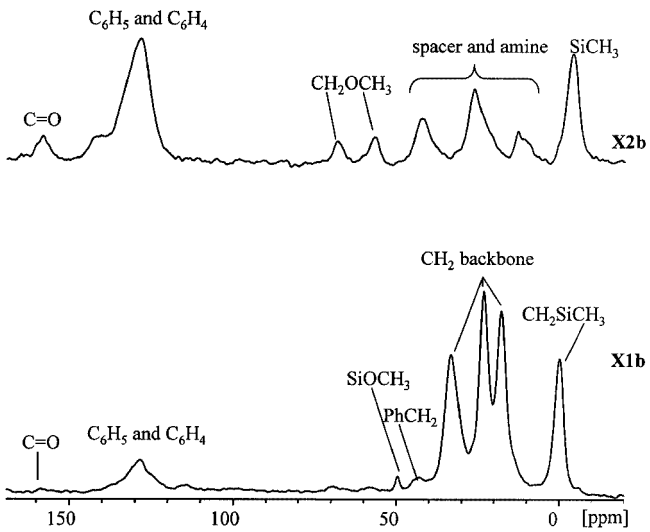

Fig. 2 ^{13}C CP/MAS NMR spectra of the polymeric materials **X1b** and **X2b** (selected).

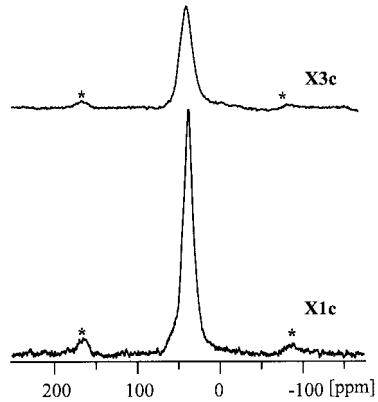

Fig. 3 ^{31}P CP/MAS NMR spectra of the polymeric materials **X1c** and **X3c** (selected). Asterisks denote spinning side bands.

EXAFS Spectroscopy

Due to the amorphous character of the polymeric materials it is impossible to attain any structural information using the conventional X-ray diffraction method. However, **EXAFS** (***E**xtended **X**-ray **A**bsorption **F**ine **S**tructure*) spectroscopy offers the possibility to investigate the coordination sphere of the reactive centers, without any limitation of the internal structure. An EXAFS analysis provides information on bond distances, coordination numbers, "Debye-Waller" factors, and the nature of the scattering atoms surrounding an excited atom [22, 23].

EXAFS measurements were carried out exemplarily on the hybrid materials **X3a** and **X3f** in the solid and suspended state (in toluene). Expectedly the experimental functions for the structural investigations of the hybrid materials in both states are quite similar. Therefore Figure 4 (EXAFS function of **X3a** in suspended state) is offered as a representative example for both complexes in the same state. The EXAFS functions of the mentioned polymeric materials in both states (Figures 5 and 6) can be described by three different atom shells for both complexes. Upon assuming two equivalent Ru−P and Ru−N bond distances, respectively, a good agreement between the calculated and experimental functions of all probed complexes was found. An additional contribution around the central ruthenium atom was established consisting of two equivalent Ru-Cl atomic distances. Structural parameters of **X3a** obtained by EXAFS (Table 2) are similar with X-ray structural data of the monomeric congener [10,13]. Only small differences were observed concerning the ruthenium−ligand bond distances. Whereas the Ru−P bond lengths are nearly equal (2.26 *vs.* 2.27 Å), the Ru−N and Ru−Cl distances differ slightly (2.19 *vs.* 2.14 Å and 2.38 *vs.* 2.45 Å, respectively). In contrast to the Ru−N bond length in **X3f** (2.08), all other distances (Ru−P and Ru−Cl) do not deviate much from **X3a** (Table 2). The differences of the bond distances of **X3a** and **X3f** in the stationary phase and in the interphase are only marginally.

SEM, EDX, and BET Measurements

Figure 7 displays the **SEM** (***S**canning **E**lectron **M**icroscopy*) images of **X1b** and **X2a**. Due to the high amount of the co-condensation agent **D°−C$_6$−D° X1b** has a rather smooth surface structure. In contrast to these findings the employment of the co-condensation agent **Me-T°** leads to an uneven surface in the case of **X2a**. From **BET** (***B**runauer-**E**mmett-**T**eller-**M**ethod*) measurements low surface areas between 2.3 and 5.94 m^2/g for **X1b − X3b** are derived.

A typical EDX (***E**nergy **D**ispersive **X**-ray analysis* [24]) spectrum of compound **X2f** is displayed in Figure 8. The K_α lines of carbon, oxygen, silicon, phosphorus, and chlorine and the L line series of ruthenium and tin are visible. An overlap occurs between the L lines of ruthenium and

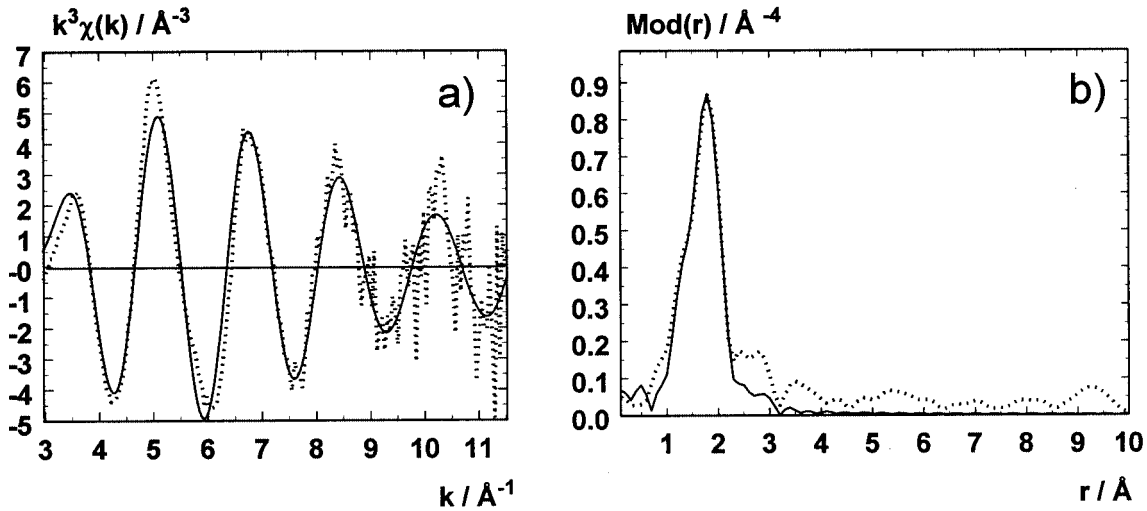

Fig. 4 Experimental (dotted line) and calculated (solid line) k^3 χ (k) functions (a) (k range: 329−14.90 $Å^{-1}$) and their Fourier transforms (b) for **X3a** in suspension with toluene (Ru-K-edge) (see Table 2 for fit parameter).

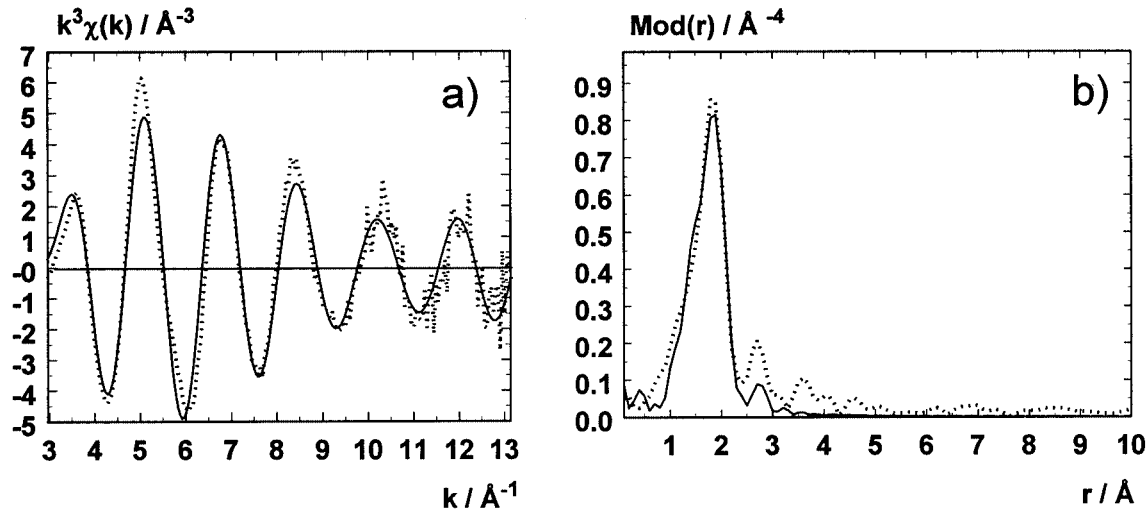

Fig. 5 Experimental (dotted line) and calculated (solid line) k^3 χ (k) functions (a) (k range: 3.40−13.30 $Å^{-1}$) and their Fourier transforms (b) for **X3a** (Ru-K-edge) (see Table 2 for fit parameter).

the K lines of chlorine. This phenomenon is corrected by peak deconvolution. Due to its high fluorescence yield, the Au-M_α line also appears under the K_β emission of phosphorus. However, the gold coating can be neglected with respect to quantification as owing to its thickness of only 20 nm additional absorption effects are not introduced. Quantification of EDX spectra was carried out using the ZAF correction procedure. This correction model is valid only for flat and homogeneous specimens. As the xerogels exhibit a pronounced morphology (see Figure 8), special care was taken to find a locally flat specimen area larger than the expected electron range which is certainly below 10 μm under the present conditions. However, several analyses of stationary phases generated by sol-gel processing have shown that this problem can be handled successfully [25].

As X-rays are strongly attenuated by the detector entrance window, EDX is not very sensitive towards the detection and quantification of light elements embedded into a matrix of higher Z material. Uncertainties in fundamental parameters and spectrometer calibration in the soft X-ray regime are an important source of error in the quantification of light elements, for which a relative error of up to 10 % has to be taken into account. In this respect, nitrogen, which is a minor constituent in all samples under investigation, is below the detection threshold and therefore has to be omitted from quantification.

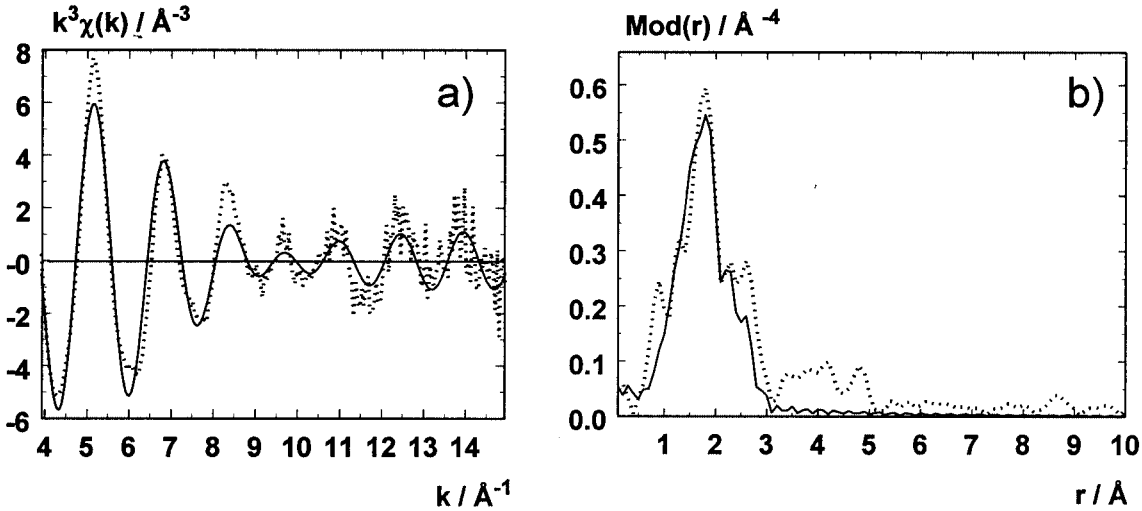

Fig. 6 Experimental (dotted line) and calculated (solid line) k^3 χ (k) functions (a) (k range: 3.29−15.00 $Å^{-1}$) and their Fourier transforms (b) for **X3f** (Ru-K-edge) (see Table 2 for fit parameter).

Table 2 EXAFS Spectroscopically Determined Structural Data of **X3a** and **X3f** in Solid and Suspension State (in Toluene)[a)]

		X3a			X3f		
		N	*r* [Å]	σ [Å]	*N*	*r* [Å]	σ [Å]
Ru−N	solid	2	2.19 ± 0.02	0.050 ± 0.008	2	2.08 ± 0.02	0.100 ± 0.015
Ru−N	suspension	2	2.15 ± 0.02	0.050 ± 0.008	2	2.08 ± 0.02	0.102 ± 0.015
Ru−P	solid	2	2.26 ± 0.02	0.050 ± 0.008	2	2.26 ± 0.02	0.122 ± 0.018
Ru−P	suspension	2	2.22 ± 0.02	0.059 ± 0.009	2	2.26 ± 0.02	0.071 ± 0.018
Ru−Cl	solid	2	2.38 ± 0.02	0.063 ± 0.016	2	2.39 ± 0.02	0.063 ± 0.016
Ru−Cl	suspension	2	2.36 ± 0.02	0.067 ± 0.017	2	2.38 ± 0.03	0.059 ± 0.015

[a)] Absorber-backscatterer distance *r*, coordination number *N*, Debye-Waller factor σ with calculated standard deviations.

Despite the numerous sources of error EDX is the only method to provide a simultaneous quantification of all present elements, including oxygen in the presence of silicon, which is usually not possible with chemical methods due to the formation of silicon carbide during the combustion process. The elemental analyses of stationary phases **X2a**, **X2b**, **X2c**, **X2f**, **X3a**, **X3e**, and **X3f** by EDX are summarized in Table 3 and compared to data obtained from the stoichiometry of the educts. These have been renormalized excluding nitrogen and hydrogen, which is a single-electron atom and thus does not emit characteristic X-rays. Finally it has to be noted that an average amount of 4 mass % tin is observed in the materials.

Hydrogenation of trans-4-Phenyl-3-butene-2-one with Interphase Catalysts X2a − X2c and *X3a − X3c*

Selected polymeric diaminediphosphineruthenium(II) complexes (**X2a − X2c** and **X3a − X3c**) were employed in the hydrogenation of the conjugated ketone Ph−CH=CH−C(O)CH_3. All reactions proceeded under mild conditions (2 bar H_2 pressure, ratio Ru(II) : KOH : Substr. = 1 : 10 : 1000, T = 35 °C, 2−propanol as solvent). From Table 4 it is derived that the tested ruthenium(II) complexes show conversions between 94 and 100 %. *trans*-4-Phenyl-3-butene-2-one is a suitable model substrate to demonstrate the selectivity of the mentioned catalysts. Either the carbonyl group (**A**) or the C=C double bond (**C**) is hydrogenated (Scheme 2). In principle also both functions (**B**) are available for hydrogenation. Catalysts **X2a**, **X3a**, **X2c**, and **X3c** with 1,2-diamines as co-ligands revealed the highest selectivities toward the formation of **A**. The remaining 1 - 6 % selectivity is equally divided between **B** and **C**. However, the selectivities of **X2b** and **X3b** with 1,3−diamines as co−ligands are much lower and were found between 50 and 55 % toward **A** (Table 4 and Scheme 2). Indeed with a selectivity between 50 % and 45 % the starting ketone was hydrogenated to give mainly **C**. These results are in agreement with the corresponding homogeneous catalysts [13].

Conclusion

Based on results which have been obtained in homogeneous phase the interphase catalysts **X1a − X1c**, **X2a − X2g**, and **X3a − X3g**, are expected to be active in the hydrogenation of unsaturated ketones. As a precondition, the reactive cen-

Table 3 Elemental Analysis of Compounds **X2a** − **X2c**, **X2f**, **X3a**, **X3e**, and **X3f** by EDX

Xerogel	Reference data[a)]						EDX[b)]					
	Composition [%]						Composition [%]					
	C	O	P	Si	Cl	Ru	C	O	P	Si	Cl	Ru
X2a	40.4	22.8	4.0	21.7	4.6	6.5	40.7	21.2	4.8	23.2	3.0	7.1
X2b	40.8	22.6	4.0	21.6	4.5	6.5	39.4	19.0	5.6	24.3	3.5	8.2
X2c	40.8	22.6	4.0	21.6	4.5	6.5	34.8	16.7	6.3	28.7	4.4	9.1
X2f	45.0	21.0	3.7	20.1	4.2	6.0	41.9	11.4	5.3	27.1	4.1	10.2
X3a	34.1	27.1	2.8	28.2	3.2	4.6	44.3	21.5	4.1	23.5	2.0	4.6
X3e	36.9	25.9	2.7	27.0	3.1	4.4	36.0	24.0	3.7	28.8	2.3	5.2
X3f	37.1	25.8	2.7	26.9	3.1	4.4	40.4	18.2	4.4	27.3	3.0	6.7

[a)] Derived from the stoichiometry of the educts, excluding hydrogen and nitrogen (see text for explanation). [b)] Quantified by the ZAF correction procedure.

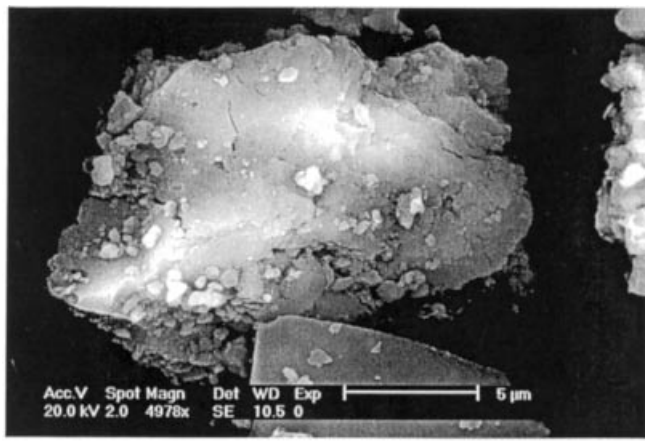

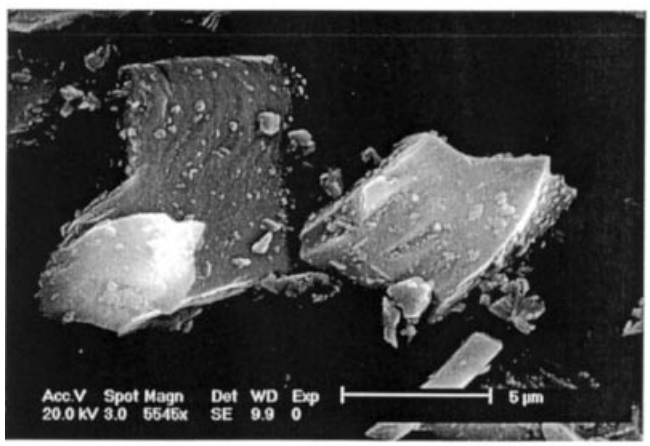

Fig. 7 Scanning electron micrographs of **X2a** (top) and **X1b** (bottom).

ters have to be accessible for the substrates, which is mainly achieved by swelling the processed polymeric materials in appropriate solvents to form interphase systems. Essentially the accessibility depends on the mobility of the entire polymeric matrix and hence on the type and amount of co-condensation agents [17]. Therefore in this investigation $CH_3Si(OCH_3)_3$ (**Me−T°**) and $(MeO)_2SiMe-(CH_2)_6-MeSi(OMe)_2$ (**D°−C$_6$−D°**) were used. As could be demonstrated [26] T-silyl functionalized materials are provided with somewhat higher BET values by which the accessibility is enhanced compared to those having D-silyl groups.

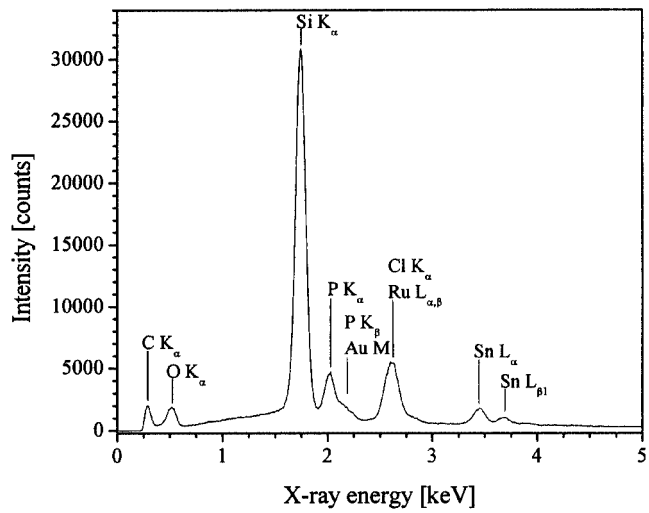

Fig. 8 Typical energy-dispersive X-ray spectrum of **X2f** generated by electrons with a primary beam energy of 20 keV. Peaks are assigned to the characteristic X-ray emission lines. For the occurrence of gold and the absence of nitrogen refer to text.

The monomeric ruthenium(II) precursor complexes were provided with T-silyl functions to increase the cross linkage of the poly-co-condensates. Such an anchoring to the polymeric carrier matrix suppresses the leaching problem that could arise and increase both the surface area and the stability of the polymeric materials. Selected interphase catalysts which are introduced in this investigation are part of an array of catalysts which show a high degree of activity and selectivity in the hydrogenation of *trans*-4-phenyl-3-butene-2-one under mild conditions.

Experimental Part

General Comments

CP/MAS solid-state NMR spectra were recorded on Bruker DSX 200 (4.7 T) and Bruker ASX 300 (7.05 T) multinuclear spec-

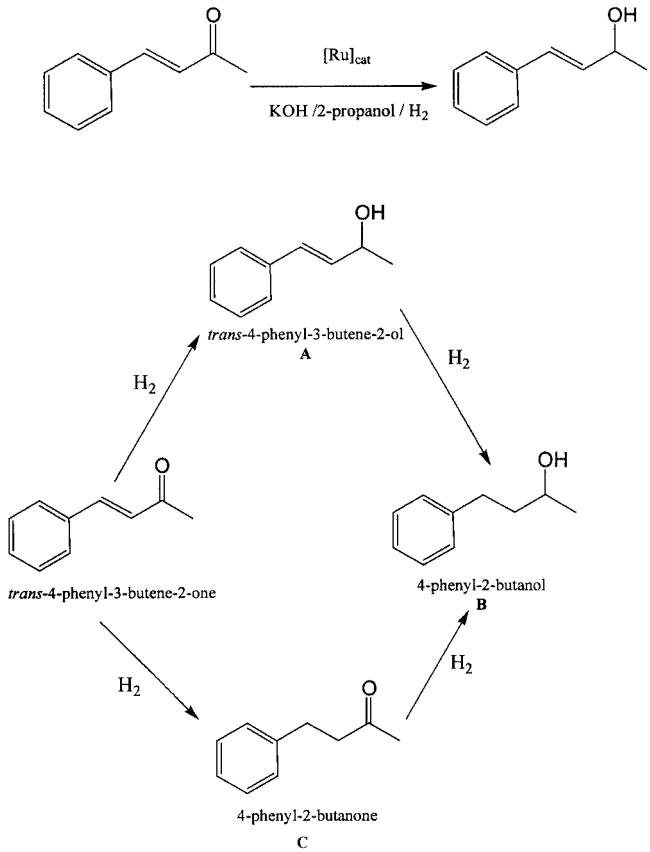

Scheme 2 Different hydrogenation possibilities of *trans*-4-phenyl-3-butene-2-one as a model substrate.

Table 4 Catalytic Hydrogenation of *trans*-4-Phenyl-3-butene-2-one

Complexes	Conversion (%)	Time (h)	Selectivity (%)[a]
X2a	100	48	94
X3a	94	48	95
X2b	98	48	55
X3b	98	48	50
X2c	100	35	99
X3c	98	48	96

[a] Selectivity toward C=O hydrogenation.

trometers equipped with wide-bore magnets. Magic angel spinning was applied at 4 kHz (^{29}Si) and 10 kHz (^{13}C, ^{31}P) using (4 mm ZrO_2 rotors). Frequencies and standards: ^{31}P, 81.961 MHz (4.7 T), 121.442 MHz (7.05 T) [85 % H_3PO_4, $NH_4H_2PO_4$ (δ = 0.8) as second standard]; ^{13}C, 50.228 MHz (4.7 T), 75.432 MHz (7.05 T) [TMS, carbonyl resonance of glycine (δ = 176.05) as second standard]; ^{29}Si, 39.73 MHz (4.7 T), 59.595 MHz (7.05 T, (Q8M8 as second standard). All samples were packed under exclusion of molecular oxygen. IR data were obtained on a Bruker IFS 48 FT−IR spectrometer. The analyses of the hydrogenation experiments were performed on a GC 6000 Vega Series 2 (Carlo Erba Instrument) with an FID and capillary column PS 255 [10 m, carrier gas , He (40 kPa), integrator 3390 A (Hewlett Packard)].

The EXAFS measurements were performed at the ruthenium K−edge (22118 eV) at the beam line X1.1 of the Hamburger Synchrotronstrahlungslabor (HASYLAB) at DESY Hamburg, under ambient conditions, energy 4.5 GeV, and initial beam current 120 mA. For harmonic rejection, the second crystal of the Si(311) double crystal monochromator was tilted to 30 %. Data were collected in transmission mode with the ion chambers flushed with argon. The energy was calibrated with a ruthenium metal foil of 20 μm thickness. The samples were prepared of a mixture of the samples and polyethylene.

Data were analyzed with a program package, specially developed for the requirements of amorphous samples [27]. The program AUTOBK of the University of Washington [27] was used for the removal of the background, and the program EXCURV92 [28] for the evaluation of the XAFS function. The resulting EXAFS function was weighted with k [29]. Data analysis in k space was performed according to the curved-wave multiple-scattering formalism of the program EXCURV92. The mean free path of the scattered electrons was calculated from the imaginary part of the potential (VPI was set to − 4.00), the amplitude reduction factor AFAC was fixed at 0.8, and an overall energy shift ΔE_o was introduced to best fit the data. In the fitting procedure the coordination numbers were at first fixed to the known values for the ligands around the ruthenium atom in all investigated complexes, and after a first iteration of the bond distances and "Debye Waller" factors varied.

Scanning electron microscopy was performed on a XL 30 scanning electron microscope by *Philips* equipped with an DX-4 energy dispersive X-ray detection system by *EDAX*. This consists of a liquid nitrogen cooled lithium-drifted silicon detector with an active area of 10 mm^2 and the eDXi 2.11 software package. The detector resolution is 149 eV at Mn-K_α (5.984 keV) and the sample-detector distance is 50 mm at a take-off angle of 35° in the present system. The sample powder was placed on a commercial specimen stub covered with an adhesive tab and subsequently provided with a sputtered 20 nm gold layer to ensure conductivity. The primary beam energy was 20 keV during all investigations. A probe current of 192 pA was applied for recording electron micrographs, whereas X-ray emission spectra were acquired under spot illumination applying a probe current of 569 pA for 400 live seconds. Under these conditions, count rates of 2000-3000 counts per second at dead times of approximately 33 % are achieved with the present compounds. Measurements were repeated several times at various specimen positions to ensure reproducibility. Quantification of X-ray spectra was carried out employing the ZAF correction procedure [30−32] after subtraction of the Bremsstrahlung background.

The surface areas were determined by analyzing the N_2 adsorption isotherm according to the BET method using Micromeritics Gemini. All manipulations were performed under an atmosphere of argon by employing usual Schlenk techniques. All solvents were dried according to common procedures, distilled and stored under argon. The T−silyl functionalized ruthenium complexes were synthesized as described in a previous paper [16]. The co-condensation agent **D°−C$_6$−D°** was synthesized according to the literature [33]. Me−Si(OMe)$_3$ and (n−Bu)$_2$Sn(OAc)$_2$ were purchased from Fluka and Merck, respectively, and stored under argon.

General Procedure for Sol−Gel Processing

To a solution of **1a(T°) − 1g(T°)** in 5 ml of MeOH and 15 ml of THF the corresponding amount of the co-condensation agent **D°−C$_6$**−D° or **Me−T°**, H_2O, and 100 μl of (n−Bu)$_2$Sn(OAc)$_2$ were added. After 3 d stirring at room temperature, the precipitated gel was washed with 10 ml of toluene and diethyl ether each, and 15 ml

of petroleum ether (40 − 70). Finally the xerogels were grinded and dried under vacuum for 24 h.

X1a: **1aT°** (300 mg, 0.235 mmol) and **D°−C$_6$−D°** (692 mg, 2.35 mmol) were sol−gel processed with water (600 µl, 33.3 mmol). After work up 420 mg (87 %) of a pale yellow powder was obtained.
$C_{202}H_{420}Cl_2N_6O_{22}P_2RuSi_{42}$: calcd C 47.58, H 8.30, N 1.65 %; found C 43.54, H 7.99, N 0.95 %.

^{31}P CP/MAS NMR: δ = 37.6. ^{13}C CP/MAS NMR: δ = −0.4 ($SiCH_3$), 17.6, 22.8, 33.4 (CH_2 of co-condensation agent and spacer), 49.5 ($SiOCH_3$), 128.7, 139.0 (br, C−phenyl). ^{29}Si CP/MAS NMR: δ = −2.4 (D°), −12.8 (D^1), −22.5 (D^2), −58.1(T^2), −67.2 (T^3). IR (KBr, cm^{-1}): ν(C=O) 1559, 1663. N_2 surface area: 2.31 m^2 g^{-1}.

X1b: 1bT° (300 mg, 0.233 mmol) and **D°−C$_6$−D°** (686 mg, 2.33 mmol) were sol−gel processed with water (600 µl, 33.3 mmol). After working up 438 mg (90 %) of a pale yellow powder was obtained.
$C_{203}H_{422}Cl_2N_6O_{22}P_2RuSi_{42}$: calcd C 47.69, H 8.32, N 1.64 %; found C 44.45, H 7.83, N 0.98 %.

^{31}P CP/MAS NMR: δ = 39.7. ^{13}C CP/MAS NMR: δ = −0.3 ($SiCH_3$), 17.6, 23.1, 33.1 (CH_2 of co-condensation agent and spacer), 43.0 ($PhCH_2$, C(O)NH*C*H$_2$), 49.5 ($SiOCH_3$), 58.0 (OCH_3), 69.3 (CH_2O), 158.6 (C=O), 128.7 (br, C−phenyl). ^{29}Si CP/MAS NMR: δ = −2.3 (D°), −13.1 (D^1), −22.6 (D^2), −58.2(T^2), −68.1 (T^3). IR (KBr, cm^{-1}): ν(C=O) 1556, 1659. N_2 surface area: 3.09 m^2 g^{-1}.

X1c: 1cT° (300 mg, 0.233 mmol) and **D°−C$_6$−D°** (686 mg, 2.33 mmol) were sol−gel processed with water (600 µl, 33.3 mmol). After working up 450 mg (93 %) of a pale yellow powder was obtained.
$C_{203}H_{422}Cl_2N_6O_{22}P_2RuSi_{42}$: calcd C 47.69, H 8.32, N 1.64 %; found C 43.35, H 8.14, N 0.98 %.

^{31}P CP/MAS NMR: δ = 38.1. ^{13}C CP/MAS NMR: δ = −5.8 (($H_3CO)_2$Si-*C*H$_3$), −0.3 ($SiCH_3$), 17.6, 23.1, 33.1 (CH_2 of co-condensation agent and spacer), 42.7 ($PhCH_2$, C(O)NH*C*H$_2$), 49.5 ($SiOCH_3$), 57.7 (OCH_3), 69.3 (CH_2O), 159.0 (C=O), 128.7 (br, C−phenyl). ^{29}Si CP/MAS NMR: δ = −1.9 (D°), −14.2 (D^1), −22.5 (D^2), −58.5(T^2), −67.7 (T^3). IR (KBr, cm^{-1}): ν(C=O) 1569, 1653.

X2a: 1aT° (300 mg, 0.235 mmol) and **Me−T°** (320 mg, 2.35 mmol) were sol−gel processed with water (300 µl, 16.6 mmol). After working up 333 mg (82 %) of a pale yellow powder was obtained.
$C_{52}H_{90}Cl_2N_6O_{22}P_2RuSi_{12}$: calcd C 36.26, H 5.27, N 4.88 %; found C 34.67, H 4.94, N 4.00 %

^{31}P CP/MAS NMR: δ = 37.2. ^{13}C CP/MAS NMR: δ = −3.8 ($SiCH_3$), 12.9 ($SiCH_2$, spacer), 26.2 (PCH_2, $SiCH_2CH_2$, spacer), 43.0 (C−amine, $PhCH_2$, C(O)NH*C*H$_2$), 57.1 (OCH_3), 68.7 (CH_2O), 128.4 (br, C−phenyl), 158.5 (C=O). ^{29}Si CP/MAS NMR: δ = −58.0 (T^2), −65.2 (T^3). IR (KBr, cm^{-1}): ν(C=O) 1567, 1650.

X2b: 1bT° (300 mg, 0.233 mmol) and **Me−T°** (317 mg, 2.33 mmol) were sol−gel processed with water (300 µl, 16.6 mmol). After working up 321 mg (79 %) of a pale yellow powder was obtained.
$C_{53}H_{92}Cl_2N_6O_{22}P_2RuSi_{12}$: calcd C 36.66, H 5.34, N 4.84 %; found C 35.49, H 5.58, N 4.16 %.

^{31}P CP/MAS NMR: δ = 42.2. ^{13}C CP/MAS NMR: δ = −4.1 ($SiCH_3$), 12.9 ($SiCH_2$, spacer), 26.4 (PCH_2, $SiCH_2CH_2$, spacer), 42.1 (C−amine, $PhCH_2$, C(O)NH*C*H$_2$), 56.9 (OCH_3), 68.6 (CH_2O), 128.4 (br, C−phenyl), 158.8 (C=O). ^{29}Si CP/MAS NMR: δ = −58.0 (T^2), −65.2 (T^3). IR (KBr, cm^{-1}): ν(C=O) 1567, 1651. N_2 surface area: 5.94 m^2 g^{-1}.

X2c: 1cT° (300 mg, 0.233 mmol) and **Me−T°** (317 mg, 2.33 mmol) were sol−gel processed with water (300 µl, 16.6 mmol). After working up 353 mg (87 %) of a pale yellow powder was obtained.
$C_{53}H_{92}Cl_2N_6O_{22}P_2RuSi_{12}$: calcd C 36.66, H 5.34, N 4.84 %; found C 34.00, H 4.99, N 3.78 %.

^{31}P CP/MAS NMR: δ = 38.3. ^{13}C CP/MAS NMR: δ = −4.1 ($SiCH_3$), 12.9 ($SiCH_2$, spacer), 21.5 (CH−amine), 26.2 (PCH_2, $SiCH_2CH_2$, spacer), 42.8 (C−amine, $PhCH_2$, C(O)NH*C*H$_2$), 57.4 (OCH_3), 68.7 (CH_2O), 128.4 (br, C−phenyl), 159.4 (C=O). ^{29}Si CP/MAS NMR: δ = −58.0 (T^2), −65.2 (T^3). IR (KBr, cm^{-1}): ν(C=O) 1559, 1653.

X2d: 1dT° (300 mg, 0.227 mmol) and **Me−T°** (309 mg, 2.27 mmol) were sol−gel processed with water (300 µl, 16.6 mmol). After working up 339 mg (84 %) of a brown powder was obtained.
$C_{56}H_{90}Cl_2N_6O_{22}P_2RuSi_{12}$: calcd C 37.99, H 5.12, N 4.75 %; found C 36.55, H 4.26, N 3.83 %.

^{31}P CP/MAS NMR: δ = 44.1. ^{13}C CP/MAS NMR: δ = −3.9 ($SiCH_3$), 12.9 ($SiCH_2$, spacer), 26.4 (PCH_2, $SiCH_2CH_2$, spacer), 43.0 ($PhCH_2$, C(O)NH*C*H$_2$), 57.2 (OCH_3), 68.4 (CH_2O), 128.5, 140.5 (br, C−phenyl), 158.8 (C=O). ^{29}Si CP/MAS NMR: δ = −58.0 (T^2), −65.2 (T^3). IR (KBr, cm^{-1}): ν(C=O) 1558, 1653.

X2e: 1eT° (300 mg, 0.219 mmol) and **Me−T°** (298 mg, 2.19 mmol) were sol−gel processed with water (300 µl, 16.6 mmol). After working up 290 mg (73 %) of a brown powder was obtained.
$C_{60}H_{92}Cl_2N_6O_{22}P_2RuSi_{12}$: calcd C 39.59, H 5.09, N 4.62 %; found C 37.56, H 5.38, N 3.50 %.

^{31}P CP/MAS NMR: δ = 43.9. ^{13}C CP/MAS NMR: δ = −3.8 ($SiCH_3$), 13.2 ($SiCH_2$, spacer), 26.4 (PCH_2, $SiCH_2CH_2$, spacer), 42.9 ($PhCH_2$, C(O)NH*C*H$_2$), 57.7 (OCH_3), 68.5 (CH_2O), 128.5 (br, C−phenyl), 159.2 (C=O). ^{29}Si CP/MAS NMR: δ = −58.0 (T^2), −65.3 (T^3). IR (KBr, cm^{-1}): ν(C=O) 1570, 1653.

X2f: 1fT° (300 mg, 0.219 mmol) and **Me−T°** (298 mg, 2.19 mmol) were sol−gel processed with water (300 µl, 16.6 mmol). After working up 346 mg (87 %) of a brown powder was obtained.
$C_{61}H_{93}Cl_2N_6O_{22}P_2RuSi_{12}$: calcd C 40.56, H 5.46, N 4.51 %; found C 42.11, H 4.26, N 3.84 %.

^{31}P CP/MAS NMR: δ = 29.2. ^{13}C CP/MAS NMR: δ = −3.8 ($SiCH_3$), 13.1 ($SiCH_2$, spacer), 26.6 (PCH_2, $SiCH_2CH_2$, spacer), 42.6 ($PhCH_2$, C(O)NH*C*H$_2$), 57.3 (OCH_3), 68.0 (CH_2O), 128.0 (br, C−phenyl), 158.4 (C=O). ^{29}Si CP/MAS NMR: δ = −58.0 (T^2), −65.3 (T^3). IR (KBr, cm^{-1}): ν(C=O) 1558, 1653.

X2g: 1gT° (300 mg, 0.215 mmol) and **Me−T°** (292 mg, 2.15 mmol) were sol−gel processed with water (300 µl, 16.6 mmol). After working up 297 mg (75 %) of a red powder was obtained.
$C_{63}H_{93}Cl_2N_6O_{22}P_2RuSi_{12}$: calcd C 40.74, H 5.05, N 4.52 %; found C 39.13, H 4.04, N 3.40 %.

^{31}P CP/MAS NMR: δ = 29.3. ^{13}C CP/MAS NMR: δ = −3.8 ($SiCH_3$), 12.8 ($SiCH_2$, spacer), 26.5 (PCH_2, $SiCH_2CH_2$, spacer), 42.5 ($PhCH_2$, C(O)NH*C*H$_2$), 57.3 (OCH_3), 68.9 (CH_2O), 128.9 (br, C−phenyl), 149.1 (br, C−amine), 158.1 (C=O). ^{29}Si CP/MAS NMR: δ = −58.0 (T^2), −65.3 (T^3). IR (KBr, cm^{-1}): ν(C=O) 1558, 1653.

X3a: 1aT° (300 mg, 0.235 mmol) and **Me−T°** (640 mg, 4.70 mmol) were sol−gel processed with water (600 µl, 16.6 mmol). After working up 451 mg (80 %) of a pale yellow powder was obtained.
$C_{62}H_{120}Cl_2N_6O_{37}P_2RuSi_{22}$: calcd C 31.11, H 5.05, N 3.51 %; found C 33.38, H 4.59, N 2.57 %.

^{31}P CP/MAS NMR: δ = 36.7. ^{13}C CP/MAS NMR: δ = −4.1 ($SiCH_3$), 13.1 ($SiCH_2$, spacer), 25.9 (PCH_2, $SiCH_2CH_2$, spacer), 42.7 (C−amine, $PhCH_2$, C(O)NH*C*H$_2$), 57.4 (OCH_3), 67.7 (CH_2O), 128.4, 140.0 (br, C−phenyl), 159.3 (C=O). ^{29}Si CP/MAS NMR: δ = −58.0 (T^2), −65.7 (T^3). IR (KBr, cm^{-1}): ν(C=O) 1570, 1651.

X3b: 1bT° (300 mg, 0.233 mmol) and **Me−T°** (635 mg, 4.66 mmol) were sol−gel processed with water (600 µl, 16.6 mmol). After working up 454 mg (81 %) of a pale yellow powder was obtained.
$C_{63}H_{122}Cl_2N_6O_{37}P_2RuSi_{22}$: calcd C 31.43, H 5.11, N 3.49 %; found C 33.30, H 4.33, N 2.79 %.

^{31}P CP/MAS NMR: δ = 43.6. ^{13}C CP/MAS NMR: δ = −3.6 ($SiCH_3$), 13.4 ($SiCH_2$, spacer), 26.8 (PCH_2, $SiCH_2CH_2$, spacer), 43.1 (C−amine, $PhCH_2$, C(O)NH*C*H$_2$), 57.7 (OCH_3), 68.6 (CH_2O), 128.4, 140.0 (br, C−phenyl), 159.4 (C=O). ^{29}Si CP/MAS NMR: δ = −58.0 (T^2), −64.8 (T^3). IR (KBr, cm^{-1}): ν(C=O) 1570, 1656. N_2 surface area: 4.36 m^2 g^{-1}.

X3c: 1cT° (300mg, 0.233 mmol) and **Me−T°** (635 g, 4.66 mmol) were sol−gel processed with water (600 µl, 16.6 mmol). After

working up 476 mg (85 %) of a pale yellow powder was obtained. $C_{63}H_{122}Cl_2N_6O_{37}P_2RuSi_{22}$: calcd C 31.43, H 5.11, N 3.49 %; found C 29.71, H 4.56, N 2.75 %.

^{31}P CP/MAS NMR: δ = 36.3. ^{13}C CP/MAS NMR: δ = −3.9 ($SiCH_3$), 13.2 ($SiCH_2$, spacer), 21.5 (CH−amine), 26.4 (PCH_2, $SiCH_2CH_2$, spacer), 43.1 (C−amine, $PhCH_2$, C(O)NHCH_2), 57.2 (OCH_3), 68.2 (CH_2O), 128.0 (br, C−phenyl), 158.9 (C=O). ^{29}Si CP/MAS NMR: δ = −58.0 (T^2), −65.2 (T^3). IR (KBr, cm^{-1}): ν(C=O) 1569, 1653.

X3d: 1dT° (300 mg, 0.227 mmol) and **Me−T°** (618 mg, 4.54 mmol) were sol−gel processed with water (600 µl, 16.6 mmol). After working up 478 mg (86 %) of a brown powder was obtained. $C_{66}H_{120}Cl_2N_6O_{37}P_2RuSi_{22}$: calcd C 31.47, H 4.95, N 3.44 %; found C 28.99, H 4.58, N 2.69 %.

^{31}P CP/MAS NMR: δ = 44.2. ^{13}C CP/MAS NMR: δ = −3.9 ($SiCH_3$), 13.3 ($SiCH_2$, spacer), 26.3, 22.5 (PCH_2, $SiCH_2CH_2$, spacer), 42.7 ($PhCH_2$, C(O)NHCH_2), 57.4 (OCH_3), 67.9 (CH_2O), 128.1, 140.0 (br, C−phenyl), 159.0 (C=O). ^{29}Si CP/MAS NMR: δ = −58.0 (T^2), −65.2 (T^3). IR (KBr, cm^{-1}): ν(C=O) 1572, 1656.

X3e: 1eT° (300 mg, 0.219 mmol) and **Me−T°** (597 mg, 4.38 mmol) were sol−gel processed with water (600 µl, 16.6 mmol). After working up 473 mg (87 %) of a brown powder was obtained. $C_{70}H_{122}Cl_2N_6O_{37}P_2RuSi_{22}$: calcd C 33.74, H 4.94, N 3.37 %; found C 31.99, H 3.98, N 2.30 %.

^{31}P CP/MAS NMR: δ = 42.6. ^{13}C CP/MAS NMR: δ = −3.8 ($SiCH_3$), 13.2 ($SiCH_2$, spacer), 26.4, 22.5 (PCH_2, $SiCH_2CH_2$, spacer), 43.1 ($PhCH_2$, C(O)NHCH_2), 57.3 (OCH_3), 68.4 (CH_2O), 128.4 (br, C−phenyl), 159.2 (C=O). ^{29}Si CP/MAS NMR: δ = −58.0 (T^2), −65.1 (T^3). IR (KBr, cm^{-1}): ν(C=O) 1571, 1651.

X3f: 1fT° (300 mg, 0.219 mmol) and **Me−T°** (597 mg, 4.38 mmol) were sol−gel processed with water (600 µl, 16.6 mmol). After working up 485 mg (89 %) of a brown powder was obtained. $C_{71}H_{123}Cl_2N_6O_{37}P_2RuSi_{22}$: calcd C 34.05, H 4.95, N 3.36 %; found C 31.70, H 4.20, N 2.87 %.

^{31}P CP/MAS NMR: δ = 29.4. ^{13}C CP/MAS NMR: δ = −3.7 ($SiCH_3$), 13.2 ($SiCH_2$, spacer), 22.5, 26.4 (PCH_2, $SiCH_2CH_2$, spacer), 42.7 ($PhCH_2$, C(O)NHCH_2), 57.5 (OCH_3), 67.9 (CH_2O), 128.5 (br, C−phenyl), 158.8 (C=O). ^{29}Si CP/MAS NMR: δ = −58.0 (T^2), −65.0 (T^3). IR (KBr, cm^{-1}): ν(C=O) 1570, 1653.

X3g: 1gT° (300 mg, 0.215 mmol) and **Me−T°** (586 mg, 4.30 mmol) were sol−gel processed with water (600 µl, 16.6 mmol). After working up 420 mg (78 %) of a red powder was obtained. $C_{73}H_{123}Cl_2N_6O_{37}P_2RuSi_{22}$: calcd C 34.67, H 4.90, N 3.32 %; found C 34.18, H 4.22, N 2.45 %.

^{31}P CP/MAS NMR: δ = 28.8. ^{13}C CP/MAS NMR: δ = −3.8 ($SiCH_3$), 13.3 ($SiCH_2$, spacer), 22.5, 26.6 (PCH_2, $SiCH_2CH_2$, spacer), 42.7 ($PhCH_2$, C(O)NHCH_2), 57.5 (OCH_3), 68.0 (CH_2O), 129.1 (br, C−phenyl), 149.0 (br, C−amine), 158.7 (C=O). ^{29}Si CP/MAS NMR: δ = −58.0 (T^2), −65.3 (T^3). IR (KBr, cm^{-1}): ν(C=O) 1570, 1653.

General Procedure for the Catalytic Studies

The respective diaminediphosphineruthenium(II) complex **X2a−X2c**, **X3a−X3c** (100 mg, ~6 % Ru) was placed in a 250 ml pressure Schlenk tube. Subsequently 0.06 mmol of KOH and 60 mmol of the substrate *trans*-4-phenyl-3-butene-2-one were added. The solids were stirred and warmed to approximately 50 °C during the evacuation process to remove oxygen and traces of water. Then the Schlenk tube was filled with argon gas and 80 ml of 2-propanol. Under vigorously stirring the Schlenk tube was degassed by two freeze-thaw cycles and then the suspension was sonicated for 30 min (this is important to increase the homogeneity of the mixture). Finally the reaction mixture was pressurized with 2 bar of H_2 after flushing the reaction vessel three times with H_2. The suspension was vigorously stirred at 35 °C for 2 d. During the hydrogenation process samples were taken to probe the proceeding reaction. The samples were inserted into a gas chromatograph by a special glass syringe and the reaction products were compared with authentic samples.

Acknowledgements. The support of this research by the Deutsche Forschungsgemeinschaft (Graduiertenkolleg 'Chemie in Interphasen', Grant No 441/01−2, Bonn, Bad Godesberg) and by the Fonds der Chemischen Industrie, Frankfurt/Main is gratefully acknowledged.

References

[1] E. Lindner, H. A. Mayer, I. Warad, K. Eichele, *J. Organomet. Chem.*, in press.
[2] P. Seneci, *Solid-Phase Synthesis and Combinatorial Technologies*, Wiley, New York, 2000.
[3] G. Jung, *Combinatorial Chemistry: Synthesis, Analysis, Screening*, Wiley, Weinheim, 1999.
[4] U. Grether, H. Waldmann, *Angew. Chem. Int. Ed.* **2000**, *39*, 1629.
[5] H. E. Tuinstra, C. H. Cummins, *Adv. Mater.* **2000**, *12*, 1819.
[6] B. Jandeleit, D. J. Schaefer, T. S. Powers, H. W. Turner, W. H. Weinberg, *Angew. Chem. Int. Ed.* **1999**, *38*, 2495.
[7] R. Schlögl, *Angew. Chem. Int. Ed.* **1998**, *37*, 2333.
[8] A. Holzwarth, H. Schmidt, W. F. Maier, *Angew. Chem. Int. Ed.* **1998**, *37*, 2644.
[9] K. D. Shimizu, M. L. Snapper, A. H. Hoveyda, *Chem. Eur. J.* **1998**, *4*, 1885.
[10] C. Nachtigal, S. Al-Gharabli, K. Eichele, E. Lindner, H. A. Mayer, *Organometallics* **2002**, *21*, 105.
[11] R. Noyori, T. Ohkuma, *Angew. Chem. Int. Ed.* **2001**, *40*, 40.
[12] M. Yamakawa, H. Ito, R. Noyori, *J. Am. Chem. Soc.* **2001**, *122*, 1466.
[13] E. Lindner, I. Warad, K. Eichele, H. A. Mayer, *Inorg. Chim. Acta*, in press.
[14] E. Lindner, T. Schneller, F. Auer, H. A. Mayer, *Angew. Chem. Int. Ed.* **1999**, *38*, 2154.
[15] Z. Lu, E. Lindner, H. A. Mayer, *Chem. Rev.* **2002**, *102*, 3543.
[16] E. Lindner, S. Al-Gharabli, H. A. Mayer, *Inorg. Chim. Acta* **2002**, *334*, 113.
[17] E. Lindner, A. Baumann, P. Wegner, H. A. Mayer, U. Reinöhl, A. Weber, T. S. Ertel, H. Bertagnolli, *J. Mater. Chem.* **2000**, *10*, 1655.
[18] E. Holder, D. Oelkrug, H. Egelhaaf, H. A. Mayer, E. Lindner, *J. Fluorescence*, in press.
[19] J. C. Brinker, W. G. Scherer, *Sol Gel Science*, Academic Press, London, 1990.
[20] G. E. Maciel, D. W. Sindorf, *J. Am. Chem. Soc.* **1980**, *102*, 7607.
[21] C. A. Fyfe, *Solid State NMR for Chemists*, CRC Press, Gulph, ON, 1984.
[22] E. A. Stern, *Phys. Rev. B* **1974**, *10*, 3027.
[23] F. W. Lytle, D. E. Sayers, E. A. Stern, *Phys. Rev. B* **1975**, *11*, 4825.
[24] L. Reimer, *Scanning Electron Microscopy*, Springer, New-York, 1998.
[25] E. Lindner, S. Brugger, S. Steinbrecher, E. Plies, M. Seiler, H. Bertagnolli, P. Wegner, H. A. Mayer, *Inorg. Chim. Acta* **2002**, *327*, 54.
[26] H. Egelhaaf, E. Holder, P. Herman, H. A. Mayer, D. Oelkrug, E. Lindner, *J. Mater. Chem.* **2001**, *11*, 2445.

[27] T. S. Ertel, H. Bertagnolli, S. Hückmann, U. Kolb, D. Peter, *Appl. Spectrosc.* **1992**, *46*, 690.
[28] M. Newville, P. Livins, Y. Yakobi, J. J. Rehr, E. A. Stern, *Phys. Rev. B* **1993**, *47*, 14126.
[29] J. S. Gurman, N. Binsted, I. Ross, *J. Phys. C* **1986**, *19*, 1845.
[30] V. D. Scott, G. Love, *X-Ray Spectrom.* **1992**, *21*, 27.
[31] J. Wernisch, *X-Ray Spectrom.* **1985**, *14*, 109.
[32] C. Poehn, J. Wernisch, W. Hanke, *X-Ray Spectrom.* **1985**, *14*,120.
[33] E. Lindner, T. Schneller, H. A. Mayer, H. Bertagnolli, T. S. Ertel, W. Hörner, *Chem. Mater.* **1997**, *9*, 1524.